





Article

A Comparative Study of Microcystin-LR Degradation by UV-A, Solar and Visible Light Irradiation Using Bare and C/N/S-Modified Titania

Tamer M. Khedr ^{1,2,3,*}, Said M. El-Sheikh ¹ , Hany M. Abdeldayem ⁴ , Adel A. Ismail ¹, Ewa Kowalska ³  and Detlef W. Bahnemann ^{2,5} 

¹ Nanomaterials and Nanotechnology Department, Central Metallurgical Research and Development Institute (CMRDI) P.O. Box: 87 Helwan, Cairo 11421, Egypt; selsheikh2001@gmail.com (S.M.E.-S.); adelali141@yahoo.com (A.A.I.)

² Institute of Technical Chemistry, Photocatalysis and Nanotechnology Research Unit, Leibniz Universität Hannover, Callinstr. 3, D-30167 Hannover, Germany; bahnemann@iftc.uni-hannover.de

³ Institute for Catalysis, Hokkaido University, N21, W10, Sapporo 001-0021, Japan; kowalska@cat.hokudai.ac.jp

⁴ Chemistry Department, Faculty of Science, Ain Shams University, 11566 Abassia, Cairo, Egypt; monamohus@yahoo.com

⁵ Laboratory Photoactive Nanocomposite Materials (Director), Saint-Petersburg State University, Ulyanovskaya str. 1, Peterhof, 198504 Saint-Petersburg, Russia

* Correspondence: khedr.t@cat.hokudai.ac.jp or ortamerkhedr56@gmail.com; Tel.: +81-11-706-9130

Received: 19 September 2019; Accepted: 20 October 2019; Published: 23 October 2019



Abstract: In an endeavor to tackle environmental problems, the photodegradation of microcystin-LR (MC-LR), one of the most common and toxic cyanotoxins, produced by the cyanobacteria blooms, was examined using nanostructured TiO₂ photocatalysts (anatase, brookite, anatase–brookite, and C/N/S co-modified anatase–brookite) under UV-A, solar and visible light irradiation. The tailoring of TiO₂ properties to hinder the electron–hole recombination and improve MC-LR adsorption on TiO₂ surface was achieved by altering the preparation pH value. The highest photocatalytic efficiency was 97% and 99% with degradation rate of 0.002 mmol L⁻¹ min⁻¹ and 0.0007 mmol L⁻¹ min⁻¹ under UV and solar irradiation, respectively, using a bare TiO₂ photocatalyst prepared at pH 10 with anatase to brookite ratio of ca. 1:2.5. However, the bare TiO₂ samples were hardly active under visible light irradiation (<25%) due to a large band gap. Upon UV, solar and vis irradiation, the complete MC-LR degradation (100%) was obtained in the presence of C/N/S co-modified TiO₂ with a degradation rate constant of 0.26 min⁻¹, 0.11 min⁻¹ and 0.04 min⁻¹, respectively. It was proposed that the remarkable activity of co-modified TiO₂ might originate from its mixed-phase composition, mesoporous structure, and non-metal co-modification.

Keywords: anatase/brookite; non-metal co-modification; emerging pollutants; cyanotoxins; microcystin-LR; photodecomposition

1. Introduction

Cyanobacteria (blue-green algae) are naturally present in aquatic environments. The increase in nutrient concentration, global water temperature, and sunlight intensity results in cyanobacterial blooms, named harmful algal blooms (HABs) [1]. It should be pointed that, besides a decrease in ecosystem stability, HABs might also cause a production of highly active toxic compounds, known as cyanotoxins, during cell lysis, which is of special concern for drinking water sources [1–3]. Moreover, the presence of cyanotoxins can increase the chemical oxygen demand, microbial growth, and disinfection

in the water distribution systems [3]. The intoxication resulting from cyanotoxins, present in drinking water, has been reported worldwide [3,4]. Cyanotoxins represent a significant threat to all living organisms on the earth since they can poison and even kill animals and humans. Additionally, they can also accumulate in various animals, such as fish and shellfish, and thus cause toxemia, such as shellfish poisoning [5]. Furthermore, an oxidative stress to plants by cyanotoxin results in tissue necrosis, influencing a proper plant growth [6]. For example, in 1996 in Brazil, 76 humans suffering from dialysis failure died because of the exposure to the high doses of cyanotoxins through polluted intravenous fluids [5,7]. In China, cyanotoxins were suspected of liver cancer resulting from drinking of polluted water [7–9]. Moreover, it was proposed that cyanotoxins-polluted water led to the development of colorectal cancer [7,10]. Cyanotoxins are classified into hepatotoxins (microcystins, nodularin), neurotoxins (anatoxins, saxitoxins, β -methylamino- L-alanine), dermatotoxins (lipopolysaccharide, lyngbyatoxins, aplysiatoxin) and cytotoxins (cylindrospermopsin) [4,7]. Microcystins (MCs), strong hepatotoxin, are considered the most widespread cyanotoxin in different environments [11,12]. So far, more than 100 variants of MCs have been identified in the environment [3]. Among them, microcystin-leucine arginine (MC-LR) is the most common and toxic [1–12]. MC-LR causes an inhibition of protein phosphatase type 1 and PP2 A, resulting in neoplasm [3]. The provisional guideline value for MCLR in drinking water should be lower than $1.0 \mu\text{g L}^{-1}$, as proposed by the World Health Organization (WHO) [13]. However, traditional water treatment processes are not sufficient for MC-LR removal [1,3,13,14]. Recently, the nanostructures photocatalysts have been considered as promising materials for environmental purification [15–25]. Among photocatalysts, nanostructure TiO_2 has been considered as one of the best photocatalysts (considering efficiency and cost) for environmental remediation, especially cyanotoxins decomposition [1,26–32]. For example, Robertson et al. reported the photodegradation of MC-LR in aqueous solution (initial conditions: concentration of 50–200 μM , pH 4, 33 °C) in the presence of TiO_2 (10 g L^{-1}) during 40 min illumination using xenon UV lamp (280 W UVASpot 400 Lamp, Uvalight Technology Ltd., Aberdeen, UK, spectral output: 330–450 nm), and they found that the initial rate of photodegradation increased with an increase of MC-LR concentration and reached $14.60 \mu\text{M min}^{-1}$ for 200 μM concentration [26]. Chen et al. examined the degradation of cylindrospermopsin (CYN) by TiO_2/UV photolysis [33]. They conducted the control experiments to investigate the role of direct photolysis, dark adsorption, photocatalytic oxidation, and oxygen in the degradation process. The influences of light intensity, TiO_2 concentration, pH value, and initial concentration of CYN were studied. It was found that CYN was completely oxidized in the presence of TiO_2 , O_2 , and UV irradiation within 10 min. The pseudo-first-order rate constants (k) increased with an increase of light intensity and TiO_2 doses, and decreased with increasing initial concentration and pH values. Despite high activity against various pollutants, TiO_2 has two main limitations: (i) electron–hole recombination, and (ii) inactivity under vis irradiation due to large band gap (e.g., ca. 3.2 eV for anatase) [1,12,14,28,31,34–36]. One of the methods for UV-activity enhancement is to form mixed-phase TiO_2 (anatase/rutile, anatase/brookite, and anatase/brookite/rutile), which might facilitate the charge transfer process (from one phase to another), thereby overcoming the recombination [37–40]. In our previous works, anatase/brookite mixed-phase TiO_2 photocatalysts were synthesized and their superior activity was found in comparison to single phase (anatase and brookite) titania samples [31,39,40]. For example, anatase, brookite, and anatase/brookite mixed-phase TiO_2 were prepared via a hydrothermal method, and used for photodegradation of cyanotoxin (cylindrospermopsin) under UV-Vis light irradiation. It was found that mixed-phase TiO_2 exhibits ~2–4 times higher photoactivity than single-phase TiO_2 [31]. On the other hand, non-metal modification allows for obtaining novel photocatalysts active also under visible light irradiation [1,3,14,28,33–50]. Triantis et al. investigated the photodegradation of MC-LR using N-modified TiO_2 , and non-modified TiO_2 (commercial Degussa P25, and reference TiO_2) photocatalysts under UV-A, solar and visible light [28]. They found that all TiO_2 photocatalysts were effective for MC-LR degradation under UV-A and solar irradiation, whereas under vis irradiation only N-modified TiO_2 was active. Recently, co-modified TiO_2 nanocatalysts have attracted significant attention because they possess a superior

photocatalytic efficiency compared to single-modified TiO₂ [1,40,42–45,47–50]. However, there are only a few reports focusing on the photodegradation of MC-LR over mesoporous A/B TiO₂ nanoparticles. In our previous reports, non-metal co-modified mesoporous anatase/brookite TiO₂ was prepared and used for photocatalytic degradation of cyanotoxins and pharmaceuticals [1,40,47,48]. For example, C/N-co-modified mesoporous anatase/brookite TiO₂ photocatalysts were highly active for MC-LR degradation under vis irradiation [1]. The impacts of initial pH value, the TiO₂ content, and MC-LR concentration on the photocatalytic activity were also investigated. It was found that the complete degradation (100%) of MC-LR (10 mg L⁻¹) was achieved, using co-modified TiO₂ (0.4 g L⁻¹) at pH 4 under visible light irradiation. Continuously, in this study, a facile method based on tuning the phase content and surface area of bare TiO₂ nanoparticles to improve the photocatalytic degradation of MC-LR was investigated. It was found that both pristine TiO₂ (prepared at pH 10), and C/N/S co-modified TiO₂ (synthesized by a simple method in which the best TiO₂ sample was calcined with thiourea) exhibited an efficient performance for the decomposition of MC-LR (C₀ = 10 mg L⁻¹, pH 4) during only 15 and 60-min irradiation with UV-A and solar simulation, respectively. In addition, the non-metal co-modified TiO₂ showed 4× higher photocatalytic activity than bare TiO₂ for MC-LR degradation during 3 h-vis irradiation.

2. Results and Discussion

2.1. Characterization of TiO₂ Photocatalysts

Six titania samples were used in this study, i.e., five non-modified samples (named as S1, S2, S3, S4 and S5) and one C/N/S-co modified sample (S4 modified with carbon, nitrogen and sulphur; named as CNS-S4). Phase structure and morphology (X-ray diffraction (XRD), and field emission scanning electron microscopy (FE-SEM); Figures 1 and 2), textural properties (specific surface area and particle size; Table 1), absorption properties (ultraviolet-visible diffuse reflectance spectroscopy (DRS); Figure 3), surface chemical characterization (X-ray photoelectron spectroscopy (XPS); Figure 4), and the photoluminescence (PL) properties of the samples were investigated. The preparation conditions, phase composition, crystallite size, specific surface area, particle size, absorption edge, and band gap of the samples are summarized in Table 1.

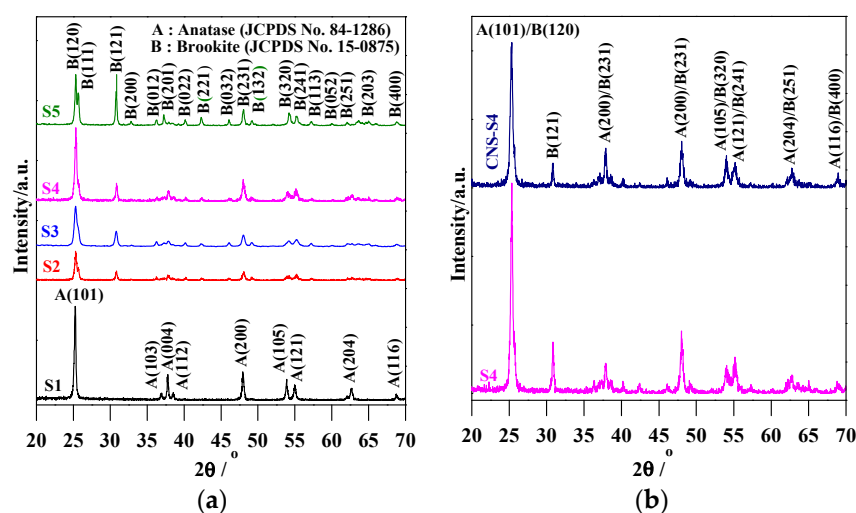


Figure 1. XRD patterns of: (a) S1, S2, S3, S4 and S5; and (b) S4 and CNS-S4.

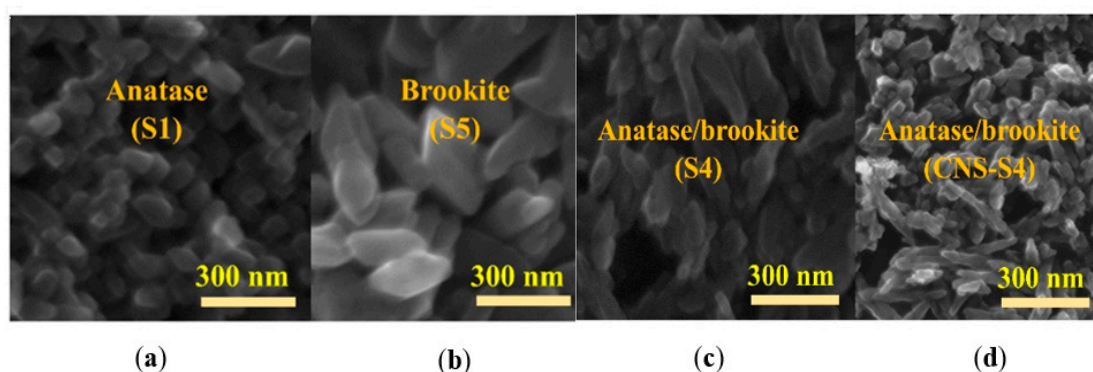


Figure 2. FE-SEM images of: (a) S1; (b) S5; (c) S4; and (d) CNS-S4.

Table 1. Preparation conditions, phase composition, crystal size, specific surface area, particle size, absorption edge and band gap of S1, S2, S3, S4, S5 and CN/S-S4 catalysts.

Sample Code	Preparation Conditions		Phase Composition		Crystal Size (nm)		Specific Surface Area (m ² g ⁻¹)	Pore Size (nm)	Absorption Edge (nm)	Band Gap (eV)
	Initial pH	Modification Source	A%	B%	A	B				
S1	3	-	100	0	29.6	-	28.0	1.12	375	3.23
S2	5	-	72.1	27.9	27.1	47.4	55.3	1.42	385	3.20
S3	7	-	65.7	34.3	25.7	46.8	60.1	1.45	389	3.18
S4	10	-	61.8	38.2	24.8	46.0	62.3	34.5	399	3.17
S5	11	-	0	100	-	52.3	23.4	1.48	374	3.30
CNS-S4	10	thiourea	70.6	27.4	28.3	48.2	30.0	2.4	420	2.90

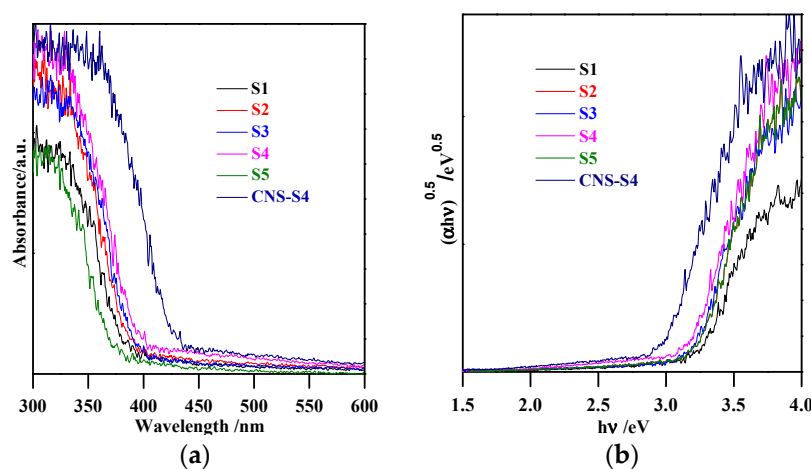


Figure 3. (a) diffuse reflectance spectra of S1, S2, S3, S4, S5 and CNS-S4; (b) curves of $(\alpha hv)^{0.5}$ versus $h\nu$.

The XRD spectra revealed that the preparation pH value (i.e., glycine/NaOH volume ratio) controlled the phase structure. The single-phase anatase (A) and brookite (B) were formed at pH 3 and 11, respectively, whereas, with pH value ranging from 5 to 10, A/B-mixed-phase TiO₂ powders were formed with a decrease in the anatase content through increasing the pH value (see Figure 1a and Table 1). Moreover, the phase structure did not change by non-metal modification, whereas the phase composition changed (anatase content increased), as shown in Figure 1b and Table 1. The crystalline size of anatase and brookite decreased within increasing of pH values (see Table 1). The specific surface area increased with increasing pH value till pH 10, and then decreased at pH 11 (Table 1). The co-modified TiO₂ (CNS-S4) and non-modified (S4) possessed a mesoporous structure, whereas the microporous structure appeared in all other samples, as shown in Table 1. Figure 2a–c shows FE-SEM for S1, S4, S5 and CNS-S4 samples, indicating that the single-phase anatase and brookite contain nano-quasi-spherical-like, and nano-spindle-like particles, respectively. In contrast, the mixed-phase TiO₂ contained nano-quasi-spherical-like anatase mixed with nano-rod-like brookite. As displayed by

UV-Vis spectroscopy, the absorption was red-shifted for the co-modified sample, reflecting that the band gap value decreased from 3.17 to 2.9 eV by non-metal modification (see Figure 3 and Table 1). The XPS spectroscopy revealed that the CNS-S4 sample was modified with C, N, and S (20.78% Ti, 58.47% O, 16.41% C, 2.5% S and 1.84% N), while the S4 sample was non-modified TiO₂ (see Figure 4). Figure 4a shows the XPS survey spectra for S4 and CNS-S4 samples. Figure 4b displays an XPS spectrum of CNS-S4 for C 1s. Three peaks were observed with binding energies of 284.8, 286.5, and 289 eV, which were ascribed to C–O and C=O, O=C–O, Ti–O–C, and C–N bonds (289 and 286.5 eV), and C–C and C–H bonds (284.8 eV) [1,40,42,43,45,47,48]. One peak with binding energy of 401 eV was obtained for nitrogen (N 1s), which was attributed to interstitial N-doping (Ti–O–N and Ti–N–O linkage), substitutional N-doping (O–Ti–N linkage), hyponitrite species, and chemisorbed N species (NO, N₂O, NO²⁻, and NO³⁻) (see Figure 4c) [1,28,34,40–45,47,48,50]. Figure 4d gives XPS spectrum of CNS-S4 for sulphur (S 2p) with binding energy of 168.6 eV, which might be assigned to S⁶⁺ 2P_{3/2} [40,42,45,46,48]. The substitution of Ti⁴⁺ by S⁶⁺ is much easier and more favorable than the replacement of O²⁻ with S²⁻ [40,48].

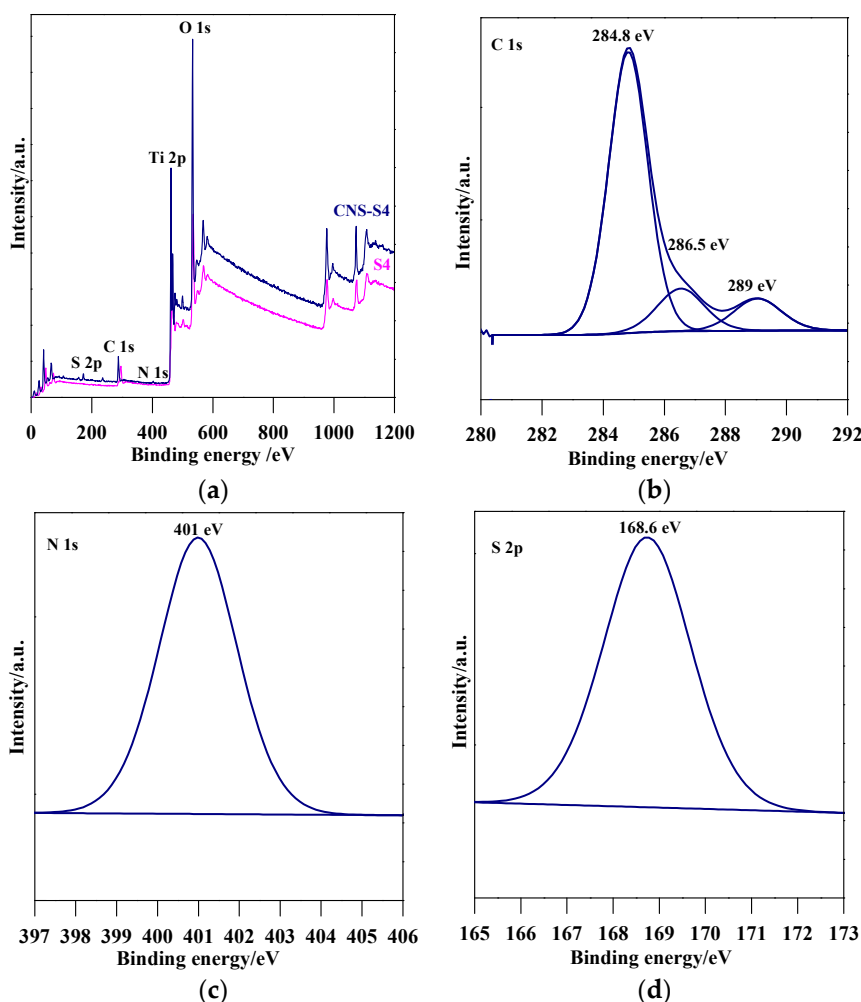


Figure 4. (a) XPS survey spectra for S4 and CNS-S4, and detailed scan in the energy regions of: (b) C 1s; (c) N 1s; and (d) S 2p of CNS-S4.

2.2. Removal of MC-LR by Adsorption and Photolysis

The experiments of MC-LR removal in the dark (absence of light) were conducted to determine the extent of MC-LR adsorption on the TiO₂ surface. Figure 5a shows the change in MC-LR concentration vs. adsorption time in the presence of non-modified TiO₂ (S1, S2, S3, S4, and S5), and non-metal-co-modified

TiO₂ (CNS-S4) catalysts. It was indicated that 3-h stirring resulted in 41%, 39%, 25%, 18%, 16%, and 14% adsorption of MC-LR on the surface of CNS-S4, S4, S3, S2, S1, and S5, respectively (see Figure 5). More efficient MC-LR adsorption on the surface of non-metal co-modified TiO₂ sample (CNS-S4) compared to the non-modified samples (Figure 5) might result from either the non-metals presence or mesoporous structure, which act as active sites for pollutants adsorption and hence improves the adsorption capacity [51–55]. Among the non-modified TiO₂, the S4 catalyst possessed the highest adsorption capacity because of its largest specific surface area (see Figure 6a).

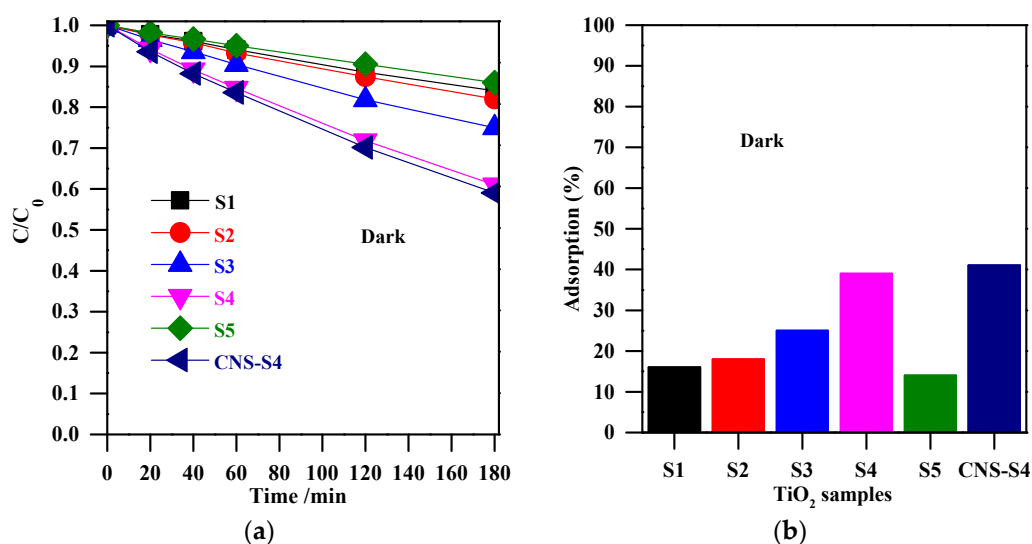


Figure 5. (a) change of the MC-LR concentration during stirring in the dark; (b) adsorption (%) for MC-LR on the surface of S1, S2, S3, S4, S5, and CNS-S4. Catalyst loading, 0.4 g L⁻¹; MC-LR dose, 10 mg L⁻¹; pH, 4; T, 25 °C; reaction volume 40 mL.

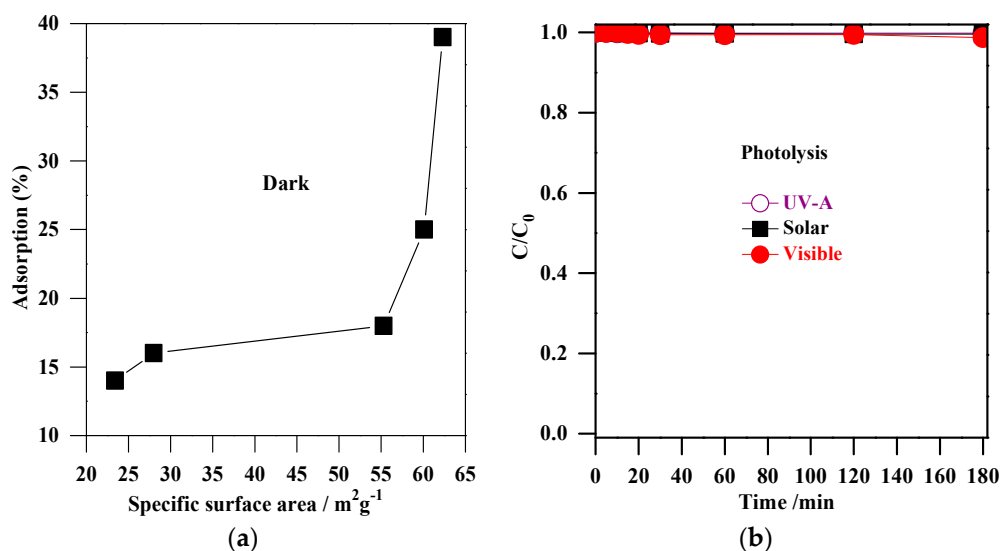


Figure 6. (a) correlation between the adsorption (%) and the specific surface areas of S1, S2, S3, S4 and S5 samples; (b) MC-LR photolysis by UV-A, solar and visible irradiation.

The direct photolysis experiments of MC-LR by UV-A, solar, and visible irradiation were carried out (after obtaining adsorption equilibrium) in an aqueous solution (Figure 6b). It was found that the MC-LR degradation by photolysis was negligible, indicating that MC-LR could not easily be removed by irradiation alone, whether UV, solar, or visible. Indeed, many reports demonstrated the radiation alone (UV, solar and visible) is not effective for elimination of MC-LR [1,3,26–28,56–64]. From the

above results, it was concluded that a more efficient method should be applied for MC-LR degradation, e.g., the photocatalysis (photocatalyst + light).

2.3. Photocatalytic Degradation of MC-LR under UV-A, Solar and Visible Light

The photocatalytic activity of the obtained TiO₂ photocatalysts was evaluated by photodegradation of MC-LR under UV-A, solar and visible light (Figures 7–10). Firstly, the discussion will focus on the photocatalytic degradation of MC-LR under UV-A and solar irradiation (Figures 7 and 8). It was found that the mixed-phase TiO₂ photocatalysts (S2, S3 and S4) were more efficient than single-phase ones (S1 and S5) toward degradation of MC-LR under UV-A (Figure 7a) and solar light (Figure 8a). The efficiency of MC-LR photodegradation under UV-A using the S4, S3, and S2 photocatalysts reached 97%, 94% and 68%, respectively, whereas only 46% and 41% were achieved in the presence of S1 and S5 photocatalysts, respectively (Figure 7c, and Table 2). The photocatalytic efficiencies of S1, S2, S3, S4 and S5 toward MC-LR degradation under solar light were slightly lower resulting in 55%, 67%, 87%, 99% and 37%, respectively (see Figure 8, and Table 2). The complete MC-LR degradation (100%) was achieved under both UV-A and solar irradiation using only co-modified TiO₂ (CNS-S4) sample (Figures 7a and 8a, and Table 2). The kinetic analysis (by plotting the natural logarithm of MC-LR concentration versus time, Figures 7b and 8b) indicates the first-order reaction, which is typical for photocatalytic decomposition of various organic compounds [1,14,31,34,39,40,43,45,48]. The estimated reaction rate constant (K) for S1, S2, S3, S4, S5 and CNS-S4 samples under UV-A irradiation were 0.041, 0.076, 0.196, 0.238, 0.035 and 0.257 min⁻¹ (Figure 7b, and Table 2), respectively, whereas, under solar irradiation, 2–6× smaller constants were obtained, i.e., 0.013, 0.019, 0.034, 0.082, 0.008 and 0.106 min⁻¹ (Figure 8b, and Table 2), respectively. The smaller reaction rate constants under solar irradiation than that under UV-A results from inactivity of bare titania under vis irradiation (main part of solar simulator emission). The corresponding reaction rates followed the order of CNS-S4 > S4 > S3 > S2 > S1 > S5 reaching 21.6 × 10⁻⁴ and 8.90 × 10⁻⁴ mmol L⁻¹ min⁻¹, 20.2 × 10⁻⁴ and 7.01 × 10⁻⁴ mmol L⁻¹ min⁻¹, 17.1 × 10⁻⁴ and 3.11 × 10⁻⁴ mmol L⁻¹ min⁻¹, 7.1 × 10⁻⁴ and 1.81 × 10⁻⁴ mmol L⁻¹ min⁻¹, 3.9 × 10⁻⁴ and 1.20 × 10⁻⁴ mmol L⁻¹ min⁻¹, and 3.3 × 10⁻⁴ and 0.76 × 10⁻⁴ mmol L⁻¹ min⁻¹ under UV-A (Figure 7c) and solar irradiation (Figure 8c), respectively.

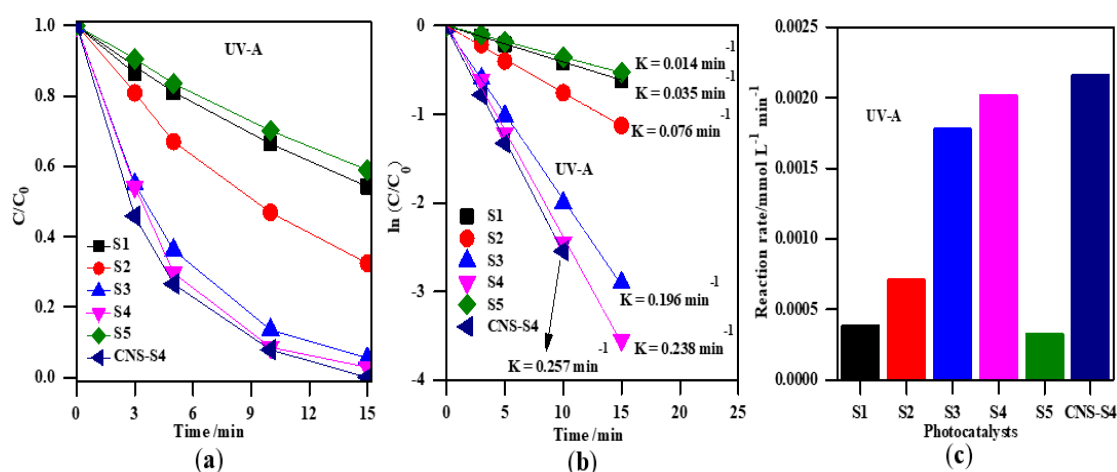


Figure 7. (a) change of the MC-LR concentration during irradiation; (b) plot of $\ln(C/C_0)$ versus irradiation time; (c) comparison of the degradation rate of MC-LR using S1, S2, S3, S4, S5, and CNS-S4 photocatalysts under UV-A light. Catalyst loading, 0.4 g L⁻¹; MC-LR dose, 10 mg L⁻¹; pH, 4; T, 25 °C; reaction volume 40 mL.

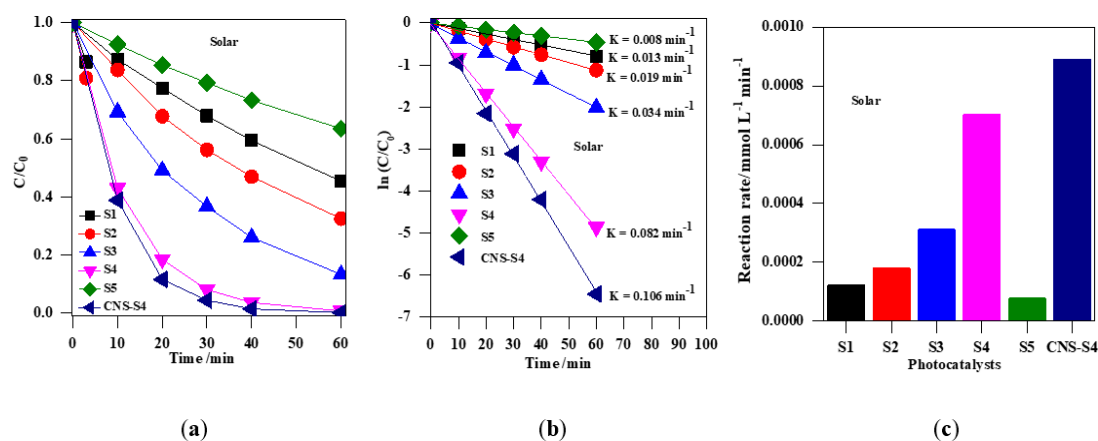


Figure 8. (a) change of the MC-LR concentration during irradiation with solar simulation; (b) plot of $\ln(C/C_0)$ versus irradiation time; (c) comparison of the degradation rate of MC-LR using S1, S2, S3, S4, S5 and CNS-S4 photocatalysts under solar irradiation. Catalyst loading, 0.4 g L^{-1} ; MC-LR dose, 10 mg L^{-1} ; pH, 4; T, $25 \text{ }^\circ\text{C}$; reaction volume 40 mL .

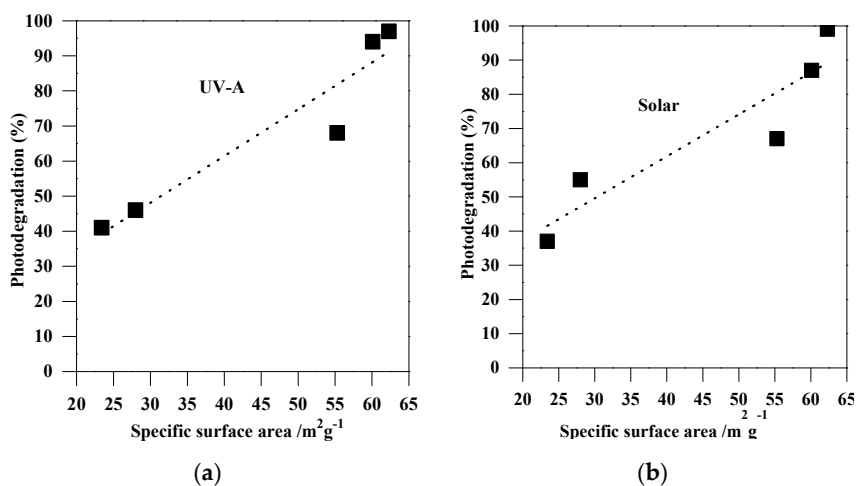


Figure 9. Correlation between the photodegradation efficiency (%) and the specific surface areas of the non-modified TiO_2 photocatalysts: (a) under UV-A; and (b) under solar irradiation.

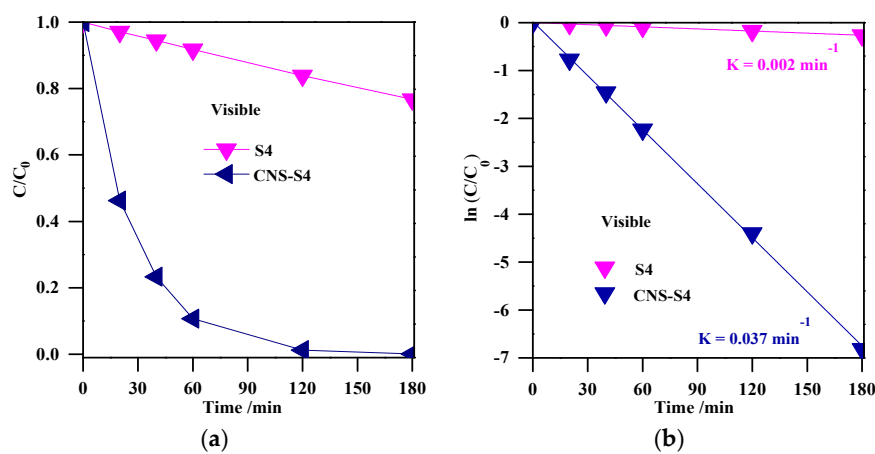


Figure 10. (a) change of the MC-LR concentration during visible light irradiation; (b) plot of $\ln(C/C_0)$ versus irradiation time. Photocatalyst loading (S4, CNS-S4), 0.4 g L^{-1} ; MC-LR dose, 10 mg L^{-1} ; pH, 4; T, $25 \text{ }^\circ\text{C}$; reaction volume 40 mL .

Table 2. The reaction rate constant (K), specific surface area (S_{BET}), reaction rate constant normalized by surface area, photodegradation efficiency, and R^2 for bare TiO_2 samples (S1, S2, S3, S4, and S5).

UVA					
Sample Code	K (min^{-1})	S_{BET} ($\text{m}^2 \text{g}^{-1}$)	K/S_{BET} ($\text{g min}^{-1} \text{m}^{-2}$) $\times 10^{-3}$	Degradation Efficiency (%)	R^2
S1	0.041	28.0	1.46	46	0.999
S2	0.076	55.3	1.37	68	
S3	0.196	60.1	3.26	94	
S4	0.238	62.3	3.82	97	
S5	0.035	23.4	1.50	41	
Solar					
Sample Code	K (min^{-1})	S_{BET} ($\text{m}^2 \text{g}^{-1}$)	K/S_{BET} ($\text{g min}^{-1} \text{m}^{-2}$) $\times 10^{-4}$	Degradation Efficiency (%)	R^2
S1	0.013	28.0	4.64	55	0.999
S2	0.019	55.3	3.44	67	
S3	0.034	60.1	5.66	87	
S4	0.082	62.3	1.32	99	
S5	0.008	23.4	3.42	37	

The remarkable photocatalytic performance of S4 (among the non-modified samples) and CNS-S4 (among all samples) might be explained by the phase structure and composition (S4 and CNS-S4), mesoporous structure (S4 and CNS-S4), high specific surface area (S4), and non-metal co-modification (CNS-S4) [1,14,28,31,34,36–51,53–55]. Both S4 and CNS-S4 contained anatase/brookite mixed-phase, and this might result in efficient separation of charge carriers by their possible migration between two phases (PL; Figure 11) [1,31,36–40,47,48]. The mesoporous structure of both S4 and CNS-S4 is also favorable for efficient activity because of providing more active sites on TiO_2 surface, the accumulation of hydroxyl radicals inside the mesopores, high dispersion of mesoporous TiO_2 in the aqueous solution, and rapid diffusion of MC-LR to the active sites on the surface of the mesoporous TiO_2 photocatalyst (as also proved by high adsorption ability) [1,31,39,40,47,48,65,66]. More efficient adsorption and degradation of MC-LR under UV-A and solar light over the S4 sample than that on the other non-modified TiO_2 samples could result from larger specific surface area, as shown in Figure 9. In order to correct the photocatalytic activity of bare TiO_2 samples (S1, S2, S3, S4, and S5) considering the surface area, the reaction rate constant was normalized by a specific surface area and summarized in Table 2. The highest photocatalytic degradation rate and normalized reaction rate constant, based on surface area, were observed for the S4 sample (with the highest surface area). Therefore, it was concluded that the surface area can play an important role in the photocatalytic degradation of MC-LR. Higher surface area introduces more active sites on the photocatalyst surface, enhancing the adsorption of organic pollutants, and it might also lead to a high concentration of surface hydroxyl groups, which can trap the photogenerated holes and thus decrease the electron–hole recombination, as demonstrated by PL results (see Figure 11) [1,31,39,40,47,66]. From the above results and discussion, it is reasonable to hypothesize that the preparation pH value is a key factor that affects directly the photocatalytic activity of the TiO_2 nanoparticles. Indeed, it is known that the pH value might control the surface characteristics and the size of aggregated nanoparticles resulting in higher content of formed hydroxyl radicals, and improved adsorption capacity of organic pollutants onto a photocatalysts surface [67]. Therefore, our results demonstrating the role of preparation pH value for controlling of the phase composition and boosting the photocatalytic activity of TiO_2 nanoparticles is consentient with previous reports [68,69]. It was also proposed that the highest activity of the co-modified TiO_2 photocatalyst (CNS-S4) results from a non-metals presence, which could act as active sites for efficient MC-LR adsorption and degradation [51–55]. It is known that non-metal modification

is responsible for the increase of superficial hydroxyl groups' content and faster electron transfer, and thus higher photocatalytic activity [1,14,28,42–45,47].

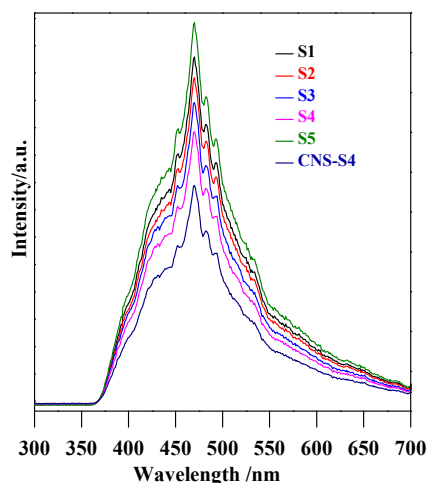


Figure 11. PL spectra of S1, S2, S3, S4, and CNS-S4 samples.

Although the results clearly showed much higher activity of CNS-S4 than other samples under solar irradiation, the reason could not be unequivocally decided, i.e., favorable surface properties, best phase composition ($A/B = 2.5$) or non-metal presence. Therefore, the photodegradation experiments under visible light irradiation were performed for two samples of the highest activity (S4 and CNS-S4), and obtained results are shown in Figure 10a. It was found that the non-modified TiO_2 photocatalyst, which could absorb only UV light ($\lambda < 400$ nm), was almost inactive ($<25\%$) under visible light irradiation, and this low MC-LR degradation might be assigned to slight light transmittance below the wavelength of 420 nm [3,28]. In contrast, MC-LR was completely degraded after 180-min stirring under visible light irradiation in the presence of C/N/S-co-modified TiO_2 (CNS-S4), as shown in Figure 10a. Similar to degradation under UV-A and solar irradiation, photocatalytic degradation of MC-LR followed first-order kinetics, as shown in Figure 10b. The rate constants and reaction rates were: $K = 0.002 \text{ min}^{-1}$, $r = 0.170 \times 10^{-4} \text{ mmol L}^{-1} \text{ min}^{-1}$ and $K = 0.037 \text{ min}^{-1}$, $r = 3.2 \times 10^{-4} \text{ mmol L}^{-1} \text{ min}^{-1}$ for S4 and CNS-S4 photocatalysts, respectively. Therefore, it was proposed that the structure and specific surface area were not the reasons for the remarkable photocatalytic activity of CNS-S4 sample under visible light irradiation. It should be pointed that these two samples possessed almost the same morphology, i.e., nano-rod-like brookite with nano-quasi-spherical-like anatase (see FE-SEM images: Figure 2c,d). In addition, although the specific surface area of CNS-S4 ($30.00 \text{ m}^2 \text{ g}^{-1}$) was two times lower than that of S4 ($62.3 \text{ m}^2 \text{ g}^{-1}$), the reaction rate of CNS-S4 was ca. 20× higher than that of S4. Therefore, it could be concluded that non-metal modification played a major role in enhancing the activity of CNS-S4 under the vis range of a solar spectrum, as clearly indicated from sample characteristics. It was proposed that the O 2p orbitals of TiO_2 could overlap with orbitals of C, N and S, forming mid-gap levels between conduction band (CB) and valence band (VB), and thus narrowing the bandgap of CNS-S4 [40,45,47,48,50]. Additionally, the carbonaceous species, which may act as a photo-sensitizer like organic dyes, might be formed on the surface of TiO_2 by carbon modification [70], whereas nitrogen might convert some Ti^{4+} to Ti^{3+} by charge compensation, and thus form donor energy levels below the conduction band [71]. The O 2p of TiO_2 could be substituted by nitrogen atoms to form isolated impurity energy levels above the valence band [70]. The photoluminescence (PL) is often a useful tool for investigating separation/recombination of photogenerated charges in semiconductors since the PL emission intensity is related directly to the electron–hole recombination rate. Lower PL emission intensities correspond to more efficient electron–hole separation and hence improve the photocatalytic activity of the photocatalyst [1,47,48]. In order to reveal the superior catalytic activity of S4 and CNS-S4 compared to the rest of the bare TiO_2 samples (S1, S2, S3, and S5), the PL spectra

with excitation wavelength of 300 nm, for all samples were conducted, and the results are shown in Figure 11. It was found that the PL spectra peaks of all samples are around 470 nm with different intensities, which decrease in the following order: CNS-S4 < S4 < S3 < S2 < S1 < S5 (see Figure 11). The higher PL intensity of single-phase TiO₂ (S1 (A), and S5 (B)) demonstrated their lower photocatalytic activity compared to mixed-phases TiO₂ (S2, S3, S4, and CNS-S4). These findings could be explained by the fact that hole trapping by non-metals and synergistic effect between anatase and brookite might facilitate the electron–hole separation [1,31,39,47,48].

3. Materials and Methods

3.1. Materials

Titanium(III) sulfate (Ti₂(SO₄)₃, Fisher, Loughborough, Leicestershire, UK, 15%), sodium nitrate (NaNO₃, Koch-light laboratories Ltd., Haverhill, Suffolk, UK, 98%), glycine (H₂N-CH₂-COOH, Sigma-Aldrich, St. Louis, MO, USA, 99%), sodium hydroxide (NaOH, LobaChemie, Pellets, Mumbai, India, 98%), thiourea (H₂N-CS-NH₂, Sigma-Aldrich, Darmstadt, Germany, 99%), MC-LR (Cal-Biochem, Nottingham, UK, 99%), and absolute ethanol (CH₃CH₂OH, Sigma-Aldrich, Darmstadt, Germany, 99.8%) were used without any further purification. The water used for the experiment was deionized water (DI, 18.2 μΩ).

3.2. Preparation and Characterization of TiO₂ Photocatalysts

The preparation and characterization of non-modified TiO₂, and C/N/S-co-modified TiO₂ were described in our previous works [39,48]. In short, to synthesize the non-modified TiO₂, with different anatase/brookite ratios, the NaNO₃ as an oxidizing agent was added to aqueous Ti₂(SO₄)₃ solution, and then stirred till formation of the colorless solution. After that, different volume ratios of glycine/NaOH were added dropwise to the colorless solution resulting in different pH values. After stirring for ~25 min, the suspension was transferred into a 100-mL Teflon-lined tube and heated at 200 °C for 20 h. Ultimately; the TiO₂ catalyst was collected, rinsed several times with DI-H₂O and alcohol, and dried at 60 °C. The samples prepared at different pH values of 3, 5, 7, 10 and 11 were named as S1, S2, S3, S4 and S5, respectively.

The N/C/S-co-modified mesoporous A/B TiO₂ photocatalyst was prepared by an ex-situ method. Shortly, the non-modified A/B mixed-phase TiO₂ powder (S4) was grounded with thiourea with a 1:1 weight ratio, and then put into a muffle furnace (Nabertherm with controller) and calcined at 450 °C for 1 h. The obtained sample was washed several times and then dried at 60 °C for 10 h. The yellow powder was signed as CNS-S4.

The obtained TiO₂ powders were characterized by various advanced methods, including X-ray diffraction (XRD, D8, Bruker AXS X-ray diffraction, Karlsruhe, Germany), field emission scanning electron microscopy (FE-SEM; QUANTA FEG 250, the Netherlands), specific surface area (SSA) measurements, ultraviolet-visible diffuse reflectance spectroscopy (UV-vis DRS, (UV-2501 PC, Shimadzu, Tokyo, Japan), and X-ray photoelectron spectroscopy (XPS, Thermo Fisher Scientific, Waltham, MA, USA).

3.3. Photocatalytic Tests

A stock aqueous solution of MC-LR (10 mg L⁻¹) was prepared (pH 6.3). Prior to the photocatalytic experiments, the standard calibration curve was made for MC-LR concentrations in the range of 5–30 mg L⁻¹. The photocatalytic degradation experiments were carried out in a double jacket round quartz reactor with a 50 mL volume. The temperature was maintained at 25 °C by the circulation of thermostated water around the reactor. Firstly, an aqueous solution of MC-LR (40 mL) was added to a round quartz reactor containing TiO₂ powder (0.4 g L⁻¹), and sonicated to obtain a uniform suspension, and then the pH value was adjusted to be 4. The reaction solution (MC-LR, H₂O, and TiO₂; pH 4) was stirred for 180 min in the dark to achieve the adsorption equilibrium for MC-LR on

the catalyst surface before starting the experiments. After that, the suspension was irradiated from the top by a UV-A lamp ($\lambda_{\max} = 365$ nm, intensity = 2 mW cm^{-2}), solar simulator lamp (SOL1200 lamp, intensity = 20 mW cm^{-2}), and visible-LED lamp ($\lambda_{\max} = 420$ nm, intensity = 1 mW cm^{-2}). The samples were taken at different times, and then filtered using a $0.22\text{-}\mu\text{m}$ filter membrane. The residual MC-LR concentration at different durations was analyzed using a high-performance liquid chromatography (HPLC, 1260, Agilent, Hamburg, Germany) with a G1311C-1260 Quat pump and a G1365D-1260 MWD UV detector (Hamburg, Germany), set at 238 nm with a C18 column (100 mm Long \times 4.6 mm i.d., $3.5 \mu\text{m}$ particles) by the method reported before [1,72]. The reaction rates were estimated and fitted with the Langmuir–Hinshelwood first-order kinetic model. The degradation rate (r) was calculated using Equation (1) [1,12,31,40]:

$$r = K \times C_0^n, \quad (1)$$

where K is the rate constant, C_0 is the initial concentration of MC-LR, and n is the order of the reaction.

The MC-LR photodegradation efficiencies (%) using the prepared TiO_2 photocatalysts under UV-A, solar and visible light were estimated using Equation (2) [9,10]:

$$\text{Photodegradation efficiency (\%)} = (1 - (C/C_0)) \times 100, \quad (2)$$

where C_0 and C are the MC-LR concentrations before and after irradiation, respectively.

4. Conclusions

The MC-LR toxin was removed from aqueous solution by UV-A, solar and visible light in the presence of nanostructured TiO_2 photocatalysts (anatase, brookite, anatase–brookite, C/N/S-co-modified anatase–brookite). A simple hydrothermal method was investigated to synthesize pristine TiO_2 nanoparticles with tunable A/B ratios, which was achieved by changing the preparation pH value. In addition, the best bare TiO_2 was calcined with thiourea to obtain C/N/S-co-modified mesoporous A/B TiO_2 . The effect of the preparation pH value on the phase composition, surface area, and photocatalytic activity was investigated, and pH-dependent behavior was observed. It was found that the single-phase TiO_2 nanoparticles, anatase and brookite, were formed at high acidic and basic pH, respectively, and A/B TiO_2 samples were obtained in the pH value range of 5 to 10. Upon increasing the pH, the specific surface areas increased, leading to higher photocatalytic activity. The co-modified and non-modified mixed-phases TiO_2 exhibited a superior photocatalytic activity compared to the single-phase TiO_2 (anatase and brookite) under UV-A and solar irradiation, probably because of mixed-phase formation, mesoporous structure, and higher specific surface area (non-modified mixed-phase TiO_2). The non-modified TiO_2 practically was inactive under visible light irradiation (<25%), whilst the complete MC-LR degradation (100%) was achieved in the presence of C/N/S co-modified- TiO_2 . It is proposed that this improved activity for co-modified TiO_2 comes from non-metal-co-modification, resulting in bandgap narrowing. Hence, highly active photocatalysts against very toxic pollutants (MC-LR) could be efficiently applied for water/wastewater purification under natural solar radiation.

Author Contributions: Conceptualization, T.M.K., S.M.E.-S., and H.M.A.; methodology, T.M.K.; experimental research, T.M.K.; data analysis, T.M.K., S.M.E.-S., H.M.A., and E.K.; writing—original draft preparation, T.M.K.; writing—review and editing, T.M.K., S.M.E.-S., A.A.I., H.M.A., and E.K.; resources, D.W.B., S.M.E.-S., A.A.I., and E.K.; publication fees, E.K.; supervision, S.M.E.-S., H.M.A., A.A.I., E.K., and D.W.B.

Funding: This work was supported by the Egyptian Ministry of Higher Education (Cultural Affairs and Missions Sector). A part of this work was also supported by the US–Egypt Joint project Cycle 17 No. 229 and short-term fellowship Cycle 6, Science & Technological Development Fund in Egypt (STDF-STF) under Grant No. 25503.

Acknowledgments: T.M.K. acknowledges the Institute of Technical Chemistry, Photocatalysis and Nanotechnology Research Unit, Leibniz Universität Hannover, Germany for hosting him during this research work.

Conflicts of Interest: The author declares no conflict of interest.

References

1. Khedr, T.M.; El-Sheikh, S.M.; Ismail, A.A.; Kowalska, E.; Bahnemann, D.W. Photodegradation of Microcystin-LR Using Visible Light-Activated C/N-co-Modified Mesoporous TiO₂ Photocatalyst. *Materials* **2019**, *12*, 1027. [[CrossRef](#)] [[PubMed](#)]
2. Chae, S.; Noeiaghahi, T.; Oh, Y.; Kim, I.S.; Park, J.-S. Effective removal of emerging dissolved cyanotoxins from water using hybrid photocatalytic composites. *Water Res.* **2019**, *149*, 421–431. [[CrossRef](#)] [[PubMed](#)]
3. Khadgi, N.; Upreti, A.R. Photocatalytic degradation of Microcystin-LR by visible light active and magnetic, ZnFe₂O₄-Ag/rGO nanocomposite and toxicity assessment of the intermediates. *Chemosphere* **2019**, *221*, 441–451. [[CrossRef](#)] [[PubMed](#)]
4. Diez-Quijada, L.; Prieto, A.I.; Guzman-Guillen, R.; Jos, A.; Camean, A.M. Occurrence and toxicity of microcystin congeners other than MC-LR and MC-RR: A review. *Food Chem. Toxicol.* **2019**, *125*, 106–132. [[CrossRef](#)]
5. Carmichael, W.W.; Azevedo, S.M.; An, J.S.; Molica, R.J.; Jochimsen, E.M.; Lau, S.K.; Rinehart, L.; Shaw, G.R.; Eaglesham, G.K. Human fatalities from cyanobacteria: Chemical and biological evidence for cyanotoxins. *Environ. Health Perspect.* **2001**, *109*, 663–668. [[CrossRef](#)]
6. Prieto, A.; Campos, A.; Camea, A. Effects on growth and oxidative stress status of rice plants (*Oryza sativa*) exposed to two extracts of toxin-producing cyanobacteria (*Aphanizomenon ovalisporum* and *Microcystis aeruginosa*). *Ecotoxicol. Environ. Saf.* **2011**, *74*, 1973–1980. [[CrossRef](#)]
7. Pantelić, D.; Svirčev, Z.; Simeunović, J.; Vidović, M.; Trajković, I. Cyanotoxins: Characteristics, production and degradation routes in drinking water treatment with reference to the situation in Serbia. *Chemosphere* **2013**, *91*, 421–441. [[CrossRef](#)]
8. Harada, K.-I.; Tsuji, K.; Watanabe, M.F.; Kondo, F. Stability of microcystins from cyanobacteria. III. Effect of pH and temperature. *Phycologia* **1996**, *35*, 83–88. [[CrossRef](#)]
9. Svirčev, Z.; Krstić, S.; Miladinov-Mikov, M.; Baltić, V.; Vidović, M. Freshwater cyanobacterial blooms and primary liver cancer epidemiological studies in Serbia. *J. Environ. Sci. Health Part C* **2009**, *27*, 36–55. [[CrossRef](#)]
10. Zhou, L.; Yu, H.; Chen, K. Relationship between microcystin in drinking water and colorectal cancer. *Biomed. Environ. Sci.* **2002**, *15*, 166–171.
11. Rastogi, R.P.; Sinha, R.P.; Incharoensakdi, A. The cyanotoxin-microcystins: Current overview. *Rev. Environ. Sci. Biotechnol.* **2014**, *13*, 215–249. [[CrossRef](#)]
12. Nawaz, M.; Moztahida, M.; Kim, J.; Shahzad, A.; Jang, J.; Miran, W.; Lee, D.S. Photodegradation of microcystin-LR using graphene-TiO₂/sodium alginate aerogels. *Carbohydr. Polym.* **2018**, *199*, 109–118. [[CrossRef](#)] [[PubMed](#)]
13. Zhang, X.; He, J.; Xiao, S.; Yang, X. Elimination kinetics and detoxification mechanisms of microcystin-LR during UV/Chlorine process. *Chemosphere* **2019**, *214*, 702–709. [[CrossRef](#)] [[PubMed](#)]
14. Wang, X.; Wang, X.; Zhao, J.; Song, J.; Zhou, L.; Wang, J.; Chen, Y. An alternative to in situ photocatalytic degradation of microcystin-LR by worm-like N, P codoped TiO₂/expanded graphite by carbon layer (NPT-EGC) floating composites. *Appl. Catal. B Environ.* **2017**, *206*, 479–489. [[CrossRef](#)]
15. Lin, Y.-F.; Hsu, Y.-J. Interfacial charge carrier dynamics of type-II semiconductor nanoheterostructures. *Appl. Catal. B Environ.* **2013**, *130*, 93–98. [[CrossRef](#)]
16. Chen, M.-Y.; Hsu, Y.-J. Type-II nanorod heterostructure formation through one-step cation exchange. *Nanoscale* **2013**, *5*, 363–368. [[CrossRef](#)]
17. Nguyen, A.T.; Lin, W.-H.; Lu, Y.-H.; Chiou, Y.-D.; Hsu, Y.-J. First demonstration of rainbow photocatalysts using ternary Cd_{1-x}Zn_xSe nanorods of varying compositions. *Appl. Catal. A* **2014**, *476*, 140–147. [[CrossRef](#)]
18. Pu, Y.-C.; Lin, W.-H.; Hsu, Y.-J. Modulation of charge carrier dynamics of Na_xH_{2-x}Ti₃O₇-Au-Cu₂O Z-scheme nanoheterostructures through size effect. *Appl. Catal. B Environ.* **2015**, *163*, 343–351. [[CrossRef](#)]
19. Chen, Y.-C.; Katsumata, K.-i.; Chiu, Y.-H.; Okada, K.; Matsushita, N.; Hsu, Y.-J. ZnO-graphene composites as practical photocatalysts for gaseous acetaldehyde degradation and electrolytic water oxidation. *Appl. Catal. A* **2015**, *490*, 1–9. [[CrossRef](#)]
20. Chen, Y.-C.; Liu, T.-C.; Hsu, Y.-J. ZnSe_{0.5}N₂H₄ Hybrid Nanostructures: A Promising Alternative Photocatalyst for Solar Conversion. *ACS Appl. Mater. Interfaces* **2015**, *7*, 1616–1623. [[CrossRef](#)]

21. Lin, W.-H.; Chiu, Y.-H.; Shao, P.-W.; Hsu, Y.-J. Metal-Particle-Decorated ZnO Nanocrystals: Photocatalysis and Charge Dynamics. *ACS Appl. Mater. Interfaces* **2016**, *8*, 32754–32763. [[CrossRef](#)] [[PubMed](#)]
22. Pua, Y.-C.; Choub, H.-Y.; Kuoc, W.-S.; Wei, K.-H.; Hsu, Y.-J. Interfacial charge carrier dynamics of cuprous oxide-reduced graphene oxide (Cu₂O-rGO) nanoheterostructures and their related visible-light-driven photocatalysis. *Appl. Catal. B Environ.* **2017**, *204*, 21–32. [[CrossRef](#)]
23. Chiu, Y.-H.; Hsu, Y.-J. Au@Cu₇S₄ yolk@shell nanocrystal-decorated TiO₂ nanowires as an all-dayactive photocatalyst for environmental purification. *Nano Energy* **2017**, *31*, 286–295. [[CrossRef](#)]
24. Kuo, M.-Y.; Hsiao, C.-F.; Chiu, Y.-H.; Lai, T.-H.; Fang, M.-J.; Wu, J.-Y.; Chen, J.-W.; Wu, C.-L.; Wei, K.-H.; Lin, H.-C.; et al. Au@Cu₂O core@shell nanocrystals as dual-functional catalysts for sustainable environmental applications. *Appl. Catal. B Environ.* **2019**, *242*, 499–506. [[CrossRef](#)]
25. Chiu, Y.-H.; Chang, T.-F.M.; Chen, C.-Y.; Sone, M.; Hsu, Y.-J. Mechanistic Insights into Photodegradation of Organic Dyes Using Heterostructure Photocatalysts. *Catalysts* **2019**, *9*, 430. [[CrossRef](#)]
26. Robertson, P.K.J.; Lawton, L.A.; Munch, B.; Rouzade, J. Destruction of cyanobacterial toxins by semiconductor photocatalysis. *Chem. Commun.* **1997**, *4*, 393–394. [[CrossRef](#)]
27. Antoniou, M.G.; Nicolaou, P.A.; Shoemaker, J.A.; de la Cruz, A.A.; Dionysiou, D.D. Impact of the morphological properties of thin TiO₂ photocatalytic films on the detoxification of water contaminated with the cyanotoxin, microcystin-LR. *Appl. Catal. B Environ.* **2009**, *91*, 165–173. [[CrossRef](#)]
28. Triantis, T.M.; Fotiou, T.; Kaloudis, T.; Kontos, A.G.; Falaras, P.; Dionysiou, D.D.; Pelaez, M.; Hiskia, A. Photocatalytic degradation and mineralization of microcystin-LR under UV-A, solar and visible light using nanostructured nitrogen doped TiO₂. *J. Hazard. Mater.* **2012**, *211*, 196–202. [[CrossRef](#)]
29. Zhang, G.; Nadagouda, M.; O’Shea, K.; El-Sheikh, S.M.; Ismail, A.A.; Likodimos, V.; Falaras, P.; Dionysiou, D.D. Degradation of Cyindrospermopsin by Using Polymorphic Titanium Dioxide under UV-Vis Irradiation. *Catal. Today* **2014**, *224*, 49–55. [[CrossRef](#)]
30. Zhang, G.; He, X.; Nadagouda, M.; O’Shea, K.; El-Sheikh, S.M.; Ismail, A.A.; Dionysiou, D.D. Identification of photocatalytic destruction intermediates and reaction pathway of cyindrospermopsin by LC/Q-TOF-ESI-MS. *Appl. Catal. B Environ.* **2015**, *163*, 591–598. [[CrossRef](#)]
31. El-Sheikh, S.M.; Khedr, T.M.; Zhang, G.S.; Vogiazzi, V.; Ismail, A.A.; O’Shea, K.; Dionysiou, D.D. Tailored synthesis of anatase-brookite heterojunction photocatalysts for degradation of cyindrospermopsin under UV-Vis light. *Chem. Eng. J.* **2017**, *310*, 428–436. [[CrossRef](#)]
32. Schneider, O.M.; Liang, R.; Bragg, L.; Jaciw-Zurakowsky, I.; Fattahi, A.; Rathod, S.; Peng, P.; Servos, M.R.; Zhou, Y.N. Photocatalytic Degradation of Microcystins by TiO₂ Using UV-LED Controlled Periodic Illumination. *Catalysts* **2019**, *9*, 181. [[CrossRef](#)]
33. Chen, L.; Zhao, C.; Dionysiou, D.D.; O’Shea, K.E. TiO₂ photocatalytic degradation and detoxification of cyindrospermopsin. *J. Photochem. Photobiol. A Chem.* **2015**, *307*, 115–122. [[CrossRef](#)]
34. Fotiou, T.; Triantis, T.; Kaloudis, T.; Hiskia, A. Photocatalytic degradation of cyindrospermopsin under UV-A, solar and visible light using TiO₂. Mineralization and intermediate products. *Chemosphere* **2015**, *119*, S89–S94. [[CrossRef](#)]
35. Fotiou, T.; Triantis, T.M.; Kaloudis, T.; O’Shea, K.E.; Dionysiou, D.D.; Hiskia, A. Assessment of the roles of reactive oxygen species in the UV and visible light photocatalytic degradation of cyanotoxins and water taste and odor compounds using C-TiO₂. *Water Res.* **2016**, *90*, 52–61. [[CrossRef](#)]
36. Hu, X.; Hu, X.J.; Tang, C.F.; Wen, S.Z.; Wu, X.F.; Long, J.; Yang, X.; Wang, H.; Zhou, L. Mechanisms underlying degradation pathways of microcystin-LR with doped TiO₂ photocatalysis. *Chem. Eng. J.* **2017**, *330*, 355–371. [[CrossRef](#)]
37. Kandiel, T.A.; Feldhoff, A.; Robben, L.; Dillert, R.; Bahnemann, D.W. Tailored titanium dioxide nanomaterials: Anatase nanoparticles and brookite nanorods as highly active photocatalysts. *Chem. Mater.* **2010**, *22*, 2050–2060. [[CrossRef](#)]
38. Shen, X.; Tian, B.; Zhang, J. Tailored preparation of titania with controllable phases of anatase and brookite by an alkaline hydrothermal route. *Catal. Today* **2013**, *201*, 151–158. [[CrossRef](#)]
39. Khedr, T.M.; El-Sheikh, S.M.; Ismail, A.A.; Bahnemann, D.W. Highly Efficient Solar Light-Assisted TiO₂ Nanocrystalline for Photodegradation of Ibuprofen Drug. *Opt. Mater.* **2019**, *88*, 117–127. [[CrossRef](#)]
40. Khedr, T.M.; El-Sheikh, S.M.; Ismail, A.A.; Bahnemann, D.W. Photodegradation of 4-aminoantipyrine over Nano-Titania Heterojunctions Using Solar and LED Irradiation Sources. *J. Environ. Chem. Eng.* **2019**, *17*, 102797. [[CrossRef](#)]

41. Matsumoto, T.; Iyi, N.; Kaneko, Y.; Kitamura, K.; Ishihara, S.; Takasu, Y.; Murakami, Y. High visible-light photocatalytic activity of nitrogen-doped titania prepared from layered titania/isostearate nanocomposite. *Catal. Today* **2007**, *120*, 226–232. [[CrossRef](#)]
42. Dong, F.; Zhao, W.; Wu, Z. Characterization and photocatalytic activities of C, N and S co-doped TiO₂ with 1D nanostructure prepared by the nano-confinement effect. *Nanotechnology* **2008**, *19*, 365–607. [[CrossRef](#)] [[PubMed](#)]
43. Liu, G.; Han, C.; Pelaez, M.; Zhu, D.; Liao, S.; Likodimos, V.; Kontos, A.G.; Falaras, P.; Dionysiou, D.D. Enhanced visible light photocatalytic activity of C N-codoped TiO₂ films for the degradation of microcystin-LR. *J. Mol. Catal. A Chem.* **2013**, *372*, 58–65. [[CrossRef](#)]
44. Andersen, J.; Han, C.; O'Shea, K.; Dionysiou, D.D. Revealing the degradation intermediates and pathways of visible light-induced NF-TiO₂ photocatalysis of microcystin-LR. *Appl. Catal. B Environ.* **2014**, *154*, 259–266. [[CrossRef](#)]
45. Zhang, G.; Zhang, Y.C.; Nadagouda, M.; Han, C.; O'Shea, K.; El-Sheikh, S.M.; Ismail, A.A.; Dionysiou, D.D. Visible light-sensitized S, N and C co-doped polymorphic TiO₂ for photocatalytic destruction of microcystin-LR. *Appl. Catal. B Environ.* **2014**, *144*, 614–621. [[CrossRef](#)]
46. Ma, D.; Xin, Y.; Gao, M.; Wu, J. Fabrication and photocatalytic properties of cationic and anionic S-doped TiO₂ nanofibers by electrospinning. *Appl. Catal. B Environ.* **2014**, *147*, 49–57. [[CrossRef](#)]
47. El-Sheikh, S.M.; Khedr, T.M.; Hakki, A.; Ismail, A.A.; Badawy, W.A.; Bahnemann, D.W. Visible Light Activated Carbon and Nitrogen Co-doped Mesoporous TiO₂ as Efficient Photocatalyst for Degradation of Ibuprofen. *Sep. Purif. Technol.* **2017**, *173*, 258–268. [[CrossRef](#)]
48. Khedr, T.M.; El-Sheikh, S.M.; Hakki, A.; Ismail, A.A.; Badawy, W.A.; Bahnemann, D.W. Highly active non-metals doped mixed-phase TiO₂ for photocatalytic oxidation of ibuprofen under visible light. *J. Photochem. Photobiol. A Chem.* **2017**, *346*, 530–540. [[CrossRef](#)]
49. Fiorenza, R.; Bellardita, M.; Scirè, S.; Palmisano, L. Effect of the addition of different doping agents on visible light activity of porous TiO₂ photocatalysts. *Mol. Catal.* **2018**, *455*, 108–120. [[CrossRef](#)]
50. Abdelraheem, W.H.M.; Patil, M.K.; Nadagouda, M.N.; Dionysiou, D.D. Hydrothermal synthesis of photoactive nitrogen- and boron- codoped TiO₂ nanoparticles for the treatment of bisphenol A in wastewater: Synthesis, photocatalytic activity, degradation byproducts and reaction pathways. *Appl. Catal. B* **2019**, *241*, 598–611. [[CrossRef](#)]
51. Ma, Y.F.; Zhang, J.L.; Tian, B.Z.; Chen, F.; Wang, L.Z. Synthesis and characterization of thermally stable Sm, N co-doped TiO₂ with highly visible light activity. *J. Hazard. Mater.* **2010**, *182*, 386–393. [[CrossRef](#)] [[PubMed](#)]
52. Nguyen, T.-B.; Hwang, M.-J.; Ryu, K.-S. High adsorption capacity of V-doped TiO₂ for decolorization of methylene blue. *Appl. Surf. Sci.* **2012**, *258*, 7299–7305. [[CrossRef](#)]
53. Marschall, R.; Wang, L. Non-metal doping of transition metal oxides for visible-light photocatalysis. *Catal. Today* **2014**, *225*, 111–135. [[CrossRef](#)]
54. Liu, S.X.; Liu, J.L.; Li, X.S.; Zhu, X.; Zhu, A.M. Gliding arc plasma synthesis of visible light active C-doped titania photocatalysts. *Plasma Process. Polym.* **2015**, *12*, 422–430. [[CrossRef](#)]
55. Li, M.; Zhang, S.; Peng, Y.; Lv, L.; Pan, B. Enhanced visible light responsive photocatalytic activity of TiO₂-based nanocrystallites: Impact of doping sequence. *RSC Adv.* **2015**, *5*, 7363–7369. [[CrossRef](#)]
56. Pinho, L.X.; Azevedo, J.; Brito, A.; Santos, A.; Tamagnini, P.; Vilar, V.J.P.; Vasconcelos, V.M.; Boaventura, R.A.R. Effect of TiO₂ photocatalysis on the destruction of *Microcystis aeruginosa* cells and degradation of cyanotoxins microcystin-LR and cylindrospermopsin. *Chem. Eng. J.* **2015**, *268*, 144–152. [[CrossRef](#)]
57. Tsuji, K.; Watanuki, T.; Kondo, F.; Watanabe, M.F.; Suzuki, S.; Nakazawa, H.; Suzuki, M.; Uchida, H.; Harada, K.-I. Stability of microcystins from cyanobacteria-II. Effect of UV light on decomposition and isomerization. *Toxicol.* **1995**, *33*, 1619–1631. [[CrossRef](#)]
58. Welker, M.; Steinberg, C. Indirect photolysis of cyanotoxins: One possible mechanism for their low persistence. *Water Res.* **1999**, *33*, 1159–1164. [[CrossRef](#)]
59. Lawton, L.; Robertson, P.; Cornish, B.; Jaspars, M. Detoxification of microcystins (cyanobacterial hepatotoxins) using TiO₂ photocatalytic oxidation. *Environ. Sci. Technol.* **1999**, *33*, 771–775. [[CrossRef](#)]
60. Lawton, L.; Robertson, P.; Cornish, B.; Marr, I.; Jaspars, M. Processes influencing surface interaction and photocatalytic destruction of microcystins on titanium dioxide photocatalysts. *J. Catal.* **2003**, *213*, 109–113. [[CrossRef](#)]

61. Van Apeldoorn, M.E.; Van Egmond, H.P.; Speijers, G.J.A.; Bakker, G.J.I. Toxins of cyanobacteria. *Mol. Nutr. Food Res.* **2007**, *51*, 7–60. [[CrossRef](#)] [[PubMed](#)]
62. Pinho, L.X.; Azevedo, J.; Vasconcelos, V.M.; Vilar, V.J.P.; Boaventura, R.A.R. Decomposition of Microcystis aeruginosa and microcystin-LR by TiO₂ oxidation using artificial UV light or natural sunlight. *J. Adv. Oxid. Technol.* **2012**, *15*, 98–106. [[CrossRef](#)]
63. Vilela, W.F.D.; Minillo, A.; Rocha, O.; Vieira, E.M.; Azevedo, E.B. Degradation of [D-Leu]-icrocystin-LR by solar heterogeneous photocatalysis (TiO₂). *Sol. Energy* **2012**, *86*, 2746–2752. [[CrossRef](#)]
64. Liao, W.; Zhang, Y.; Zhang, M.; Murugananthan, M.; Yoshihara, S. Photoelectrocatalytic degradation of microcystin-LR using Ag/AgCl/TiO₂ nanotube arrays electrode under visible light irradiation. *Chem. Eng. J.* **2013**, *231*, 455–463. [[CrossRef](#)]
65. Ismail, A.A.; Bahnemann, D.W. Mesoporous titania photocatalysts: Preparation, characterization and reaction mechanisms. *J. Mater. Chem.* **2011**, *21*, 11686–11707. [[CrossRef](#)]
66. Atitar, M.F.; Ismail, A.A.; Al-Sayari, S.A.; Bahnemann, D.; Afanasev, D.; Emeline, A.V. Mesoporous TiO₂ nanocrystals as efficient photocatalysts: Impact of calcination temperature and phase transformation on photocatalytic Performance. *Chem. Eng. J.* **2015**, *264*, 417–424. [[CrossRef](#)]
67. Jallouli, N.; Elghniji, K.; Trabelsi, H.; Ksibi, M. Photocatalytic degradation of paracetamol on TiO₂ nanoparticles and TiO₂/cellulosic fiber under UV and sunlight irradiation. *Arabian J. Chem.* **2017**, *10*, S3640–S3645. [[CrossRef](#)]
68. Lü, X.; Mao, D.; Wei, X.; Zhang, H.; Xie, J.; Wei, W. Tunable synthesis of enhanced photodegradation activity of brookite/anatase mixed-phase titanium dioxide. *J. Mater. Res.* **2013**, *28*, 400–404. [[CrossRef](#)]
69. Azeez, F.; Al-Hetlani, E.; Arafa, M.; Abdelmonem, Y.; Abdel Nazeer, A.; Amin, M.O.; Madkour, M. The effect of surface charge on photocatalytic degradation of methylene blue dye using chargeable titania nanoparticles. *Sci. Rep.* **2018**, *8*, 7104. [[CrossRef](#)]
70. Chen, D.; Jiang, Z.; Geng, J.; Wang, Q.; Yang, D. Carbon and nitrogen co-doped TiO₂ with enhanced visible-light photocatalytic activity. *Ind. Eng. Chem. Res.* **2007**, *46*, 2741–2746. [[CrossRef](#)]
71. Wang, D.-H.; Jia, L.; Wu, X.-L.; Lu, L.Q.; Xu, A.-W. One-step hydrothermal synthesis of N-doped TiO₂/C nanocomposites with high visible light photocatalytic activity. *Nanoscale* **2012**, *4*, 576–584. [[CrossRef](#)] [[PubMed](#)]
72. He, X.; Pelaez, M.; Westrick, J.A.; O’Shea, K.E.; Hiskia, A.; Triantis, T.; Kaloudis, T.; Stefan, M.I.; de la Cruz, A.A.; Dionysiou, D.D. Efficient removal of microcystin-LR by UV-C/H₂O₂ in synthetic and natural water samples. *Water Res.* **2012**, *46*, 1501–1510. [[CrossRef](#)] [[PubMed](#)]



© 2019 by the authors. Licensee MDPI, Basel, Switzerland. This article is an open access article distributed under the terms and conditions of the Creative Commons Attribution (CC BY) license (<http://creativecommons.org/licenses/by/4.0/>).